

Design improvement of a centrifugal pump for transporting salt crystals

J Q Wang¹, H Y Li¹ and X W Luo^{1*}

¹ Department of Thermal Engineering, Tsinghua University, Beijing, China.

Jiaqi19921123@hotmail.com

Abstract: This paper treats the design and optimization of a centrifugal salt-pump working under liquid-solid two phase flow condition. The design parameters are referred to a salt pump used in a salt field in Shandong Province. The design method is based on one-dimension theory, while the optimization are conducted by modifying the meridional shape and geometry parameters including wrap angle and the blade number of the pump impeller. Using the ANSYS-CFX software, and the RANS method coupled with the k- ω SST turbulence model for the simulation of liquid phase flow, while the Lagrangian Particle model for solid phase, the two-phase flow and erosion conditions are studied inside the pump. The result shows that the wrap angle and blade number have remarkable influence on the hydraulic performance, internal flow, collision risk and erosion wear conditions. Based on the numerical results, the preferable geometry parameters for salt pump design are proposed.

1. Introduction

Nowadays, hydraulic transportation technology is widely applied in China in salt industry, where salt crystals are conveyed from salt pond to salt stacks through pumps and pipes. Since there was no pump specially designed for salt transporting in the past, sewage pumps were used. To develop suitable salt pumps, it is necessary to guaranty hydraulic performance, and to improve the erosion and collision condition inside pumps.

Concerning the hydraulic performance of pumps, some improvements have been made by modifying the meridional shape and adjusting the geometrical parameters of the impeller, such as incidence angle at vane leading edge, wrap angle, vane number, etc. Bing Hao and Tan Lei studied the effects of number and thickness of blade on performance of mixed-flow pumps. They believe that the choice of blade number need considering both the power ability and the flow losses[1].Shahram Derakhshan etc. used the artificial bee colony (ABC) algorithm to improve a centrifugal pump, by changing the meridional channel and blade profile. The result shows that the ABC algorithms could be exploited as a beneficial approach in the optimal design of pumps.[2]Zhang Xiang selected wrap angle of 90°,120°,150°and 180°to study the effects of vane wrap angles on the performance of pump, finding that with the increase of wrap angle, the streamlines and blade profiles are getting similar, but the friction loss in impeller passages is getting larger, so there exists an optimum wrap angle.[3]

Besides hydraulic performance, a salt pump is faced with two major technical problems: to achieve a low percentage of particle breakage and erosion wear. Liu Juan, etc. researches the erosion and particle motion trajectory in centrifugal pump. Their result shows that the particle property has influences on the erosion situation. The solid particle with large mass was apt to move towards the



pressure surface and impacted the leading edge of impeller vane. By contrary, little particle moved to impact the rear-end surface of impeller vane near the outlet .[4] Zhao Wang, etc. conducted numerical study on sand erosion of centrifugal pump impeller, and found that with the increase of sand content the abrasion of the blade inlet increased; There was backflow at the blade inlet near the pressure surface under the working conditions of the small flow rate, and there was backflow at the blade inlet near the suction surface under large flow condition, and the abrasion increased with the increase of backflow.[5]

Although there has been a lot of researches on pump optimization and pump erosion, but there is very little to consider the situation in a salt pump. To study the effect of impeller geometry on the centrifugal pump for transporting liquid-salt crystal mixture, this paper treats hydraulic performance and erosion investigation for centrifugal pumps with different wrap angle and blade number. Based on the numerical results, this paper provides a reference for the design of high performance salt pump.

2. Calculation method

2.1. Computation domain and mesh generation

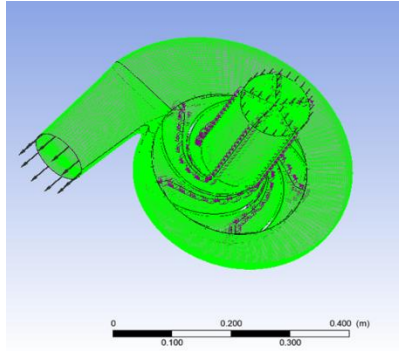
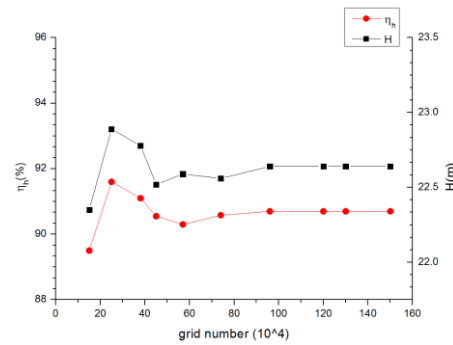
The salt pump is of centrifugal type, and designed to be operated with the flow rate of 160 m³/h at the rotational speed of 1480 r/min. The impeller diameter at the exit is 270 mm. The impeller vane width is 32 mm. The vane exit angle is 22 degrees. The diameter at pump outlet is 100mm. For comparison, six impellers with different vane wrap angle or blade number are designed, and these impellers respectively have the wrap angle of 120 degrees, 150 degrees and 180 degrees, and blade number of 4,5,6. The impeller are listed at table 1.

Table 1. Geometrical parameters for pump impellers

Impeller No.	Vane number Z	Vane angle at leading edge β_1 (°)	Vane angle at trailing edge β_2 (°)	Vane wrap angle ϕ (°)
IMP_A	5	27°	22°	120°
IMP_B	5	27°	22°	150°
IMP_C	5	27°	22°	180°
IMP_D	4	27°	22°	150°
IMP_E	5	27°	22°	150°
IMP_F	6	27°	22°	150°

Figure 1 shows the full flow passage including the volute casing impeller and inlet pipe, which is considered as the computation domain. In this paper, the structured meshes are used to discretize each computation domain, which are generated by the grid generation software ICEM-CFD.

Figure 2 shows the result for grid independence test. As shown in the figure, when the total grid number is above 1000,000, the predicted pump head and hydraulic efficiency keep almost unchanged. Thus, the numerical result is mesh independent for the mesh. In this simulation, the total mesh element number is 960,000, of which 140,000 elements for the pump inlet, 600,000 elements for the impeller, and 220,000 elements for the volute casing. In order to ensure the requirement of k- ω SST model, y plus of the grid is between 50 and 200.

**Figure 1.** Computational domain**Figure 2.** Mesh independence verification

2.2. Governing equations

Numerical simulations of the liquid-solid two-phase flow are based on the Eulerian–Lagrangian method, and the interaction between the particle and the fluid is fully coupled. [6]

2.2.1. For the liquid phase,

$$\frac{\partial \bar{u}_j}{\partial x_j} = 0 \quad (1)$$

$$\rho \frac{\partial \bar{u}_i}{\partial t} + \rho \bar{u}_j \frac{\partial \bar{u}_i}{\partial x_j} = \rho F_i + \rho F_p - \frac{\partial \bar{P}}{\partial x_i} + \mu \frac{\partial^2 \bar{u}_i}{\partial x_j \partial x_j} + \frac{\partial (-\rho \bar{u}_i \bar{u}_j)}{\partial x_j} \quad (2)$$

$$-\rho \bar{u}_i \bar{u}_j = \mu_t \left(\frac{\partial \bar{u}_i}{\partial x_j} + \frac{\partial \bar{u}_j}{\partial x_i} \right) - \frac{2}{3} \left(\rho k + \mu_t \frac{\partial \bar{u}_i}{\partial x_j} \right) \quad (3)$$

Where:

F_i is the body force, F_p is force caused by the particle, which is the counterforce of the drag force, $\mathbf{f}_p = -\frac{1}{8} \pi d_p^2 C_D \rho |\mathbf{u} - \mathbf{U}_p| (\mathbf{u} - \mathbf{U}_p)$, where $C_D = \max \left\{ \frac{24}{Re} (1 + 0.15 Re^{0.687}), 0.44 \right\}$, \mathbf{u} : fluid velocity, \mathbf{U}_p : particle velocity. δ_{ij} the kronecker delta. The shear-stress transport k- ω turbulence model are as follows:

$$\frac{\partial}{\partial t} (\rho k) + \frac{\partial}{\partial x_i} (\rho k u_i) = \frac{\partial}{\partial x_j} \left(\tau_k \frac{\partial k}{\partial x_j} \right) + \widetilde{G}_K - Y_k \quad (4)$$

$$\frac{\partial}{\partial t} (\rho w) + \frac{\partial}{\partial x_j} (\rho w u_j) = \frac{\partial}{\partial x_j} \left(\tau_w \frac{\partial w}{\partial x_j} \right) + G_w - Y_w + D_w \quad (5)$$

Where:

\widetilde{G}_K is the generation of turbulence kinetic energy due to mean velocity gradients. G_w is the generation of w . τ_k and τ_w are the effective diffusivity of k and w , respectively. Y_k and Y_w are the dissipation of k and w due to turbulence. D_w is the cross-diffusion term.

2.2.2. For the solid phase,

$$m_p \frac{d\mathbf{U}_p}{dt} = \mathbf{F}_D + \mathbf{F}_B + \mathbf{F}_R + \mathbf{F}_{VM} + \mathbf{F}_P + \mathbf{F}_{BA} \quad (6)$$

where

\mathbf{U}_p : Particle velocity.

\mathbf{F}_D : Drag force acting on the particles. $\mathbf{F}_D = \frac{1}{8} \pi d_p^2 C_D \rho_F |\mathbf{u} - \mathbf{U}_p| (\mathbf{u} - \mathbf{U}_p)$, where

$$C_D = \max \left\{ \frac{24}{Re} (1 + 0.15 Re^{0.687}), 0.44 \right\}$$

F_B : Buoyancy force due to the gravity. $F_B = \frac{\pi}{6} d_p^3 (\rho_p - \rho) g$, where d_p : Particle diameter, ρ_p :

Particle density

F_R : Force due to domain rotation, centrifugal and Coriolis forces. $F_R = m_p (-\Omega \times U_p - \Omega \times \Omega \times r_p)$

F_{VM} : Virtual or mass force.

$F_{VM} = -112\pi d_p^3 \rho_p dU/dt$

F_p : Pressure gradient force. This is the force applied on the particle due to the pressure gradient in the fluid surrounding the particle caused by fluid acceleration. It is only significant when the fluid density is comparable to or greater than the particle density.

$F_p = -m_p \nabla p$

F_{BA} : Basset force or history term which accounts for the deviation in flow pattern from a steady state.

2.3. Simulation models

In the present study, the Euler-Lagrangian method is used to simulate the liquid flow and movement of salt crystal particles based on Ansys-CFX software. The high resolution scheme is used to discretize the difference equation. The steady state turbulent flow in the salt pump is simulated using Reynolds average Navier-Stokes equations coupled with the shear-stress transport SST $k-\omega$ turbulence model. The forces acting on a salt crystal include the gravity force, buoyant force, drag force, pressure gradient force and virtual mass force. [7] Note that Basset force, a history term which accounts for the deviation in flow pattern from a steady state is not included in the present simulation due to its negligible magnitude compared to other terms.

The Finnie's model is used to analyze the erosion condition. The velocity power factor is 2.4, and the reference velocity is 585m/s according to Neopane H P. et al. [8,9]

2.4. Boundary Conditions

The boundary conditions are as follows:

- The total pressure is set at the inlet plane of the computation domain;
- A mass flow for liquid phase is assigned at the domain outlet; Several mass flow rates are set to obtain the performance curve, while the mass flow rate at design point i.e. $Q=160\text{m}^3/\text{h}$ are used for predicting the particle movement and erosion wear inside the salt pump.
- For liquid, the passage wall is set to be no slip boundary condition, while slip boundary condition is set for the solid phase. The liquid phase is saturated salt solutions (NaCl), whose density is 1330kg/m^3 and dynamic viscosity is $0.001\text{ Pa} \cdot \text{s}$.
- The solid is spherical salt crystal particles, whose diameter is 3mm, and the volume concentration is 3%, uniformly distributed in the inlet area.
- The liquid and solid phase at room temperature are used for the calculations.

3. Result and analysis

3.1. Hydraulic performance

Figure 3 shows the hydraulic performance of the pump based on numerical simulation. The simulation is under design flow condition. The results indicate that the wrap angle much affects the pump performance. With the increase of wrap angle, the input power firstly increase and then decrease slightly. While the hydraulic efficiency and head both become larger. Because with the wrap angle increases, the impeller controls the flow better, which can be seen in the internal flow analysis.

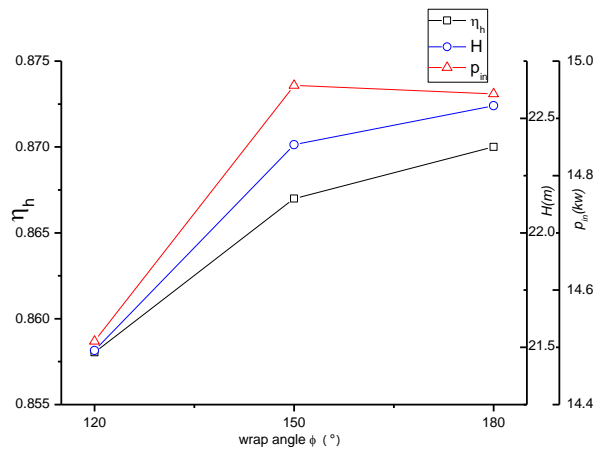


Figure 3. Hydraulic performance for pump impellers with different vane wrap angle

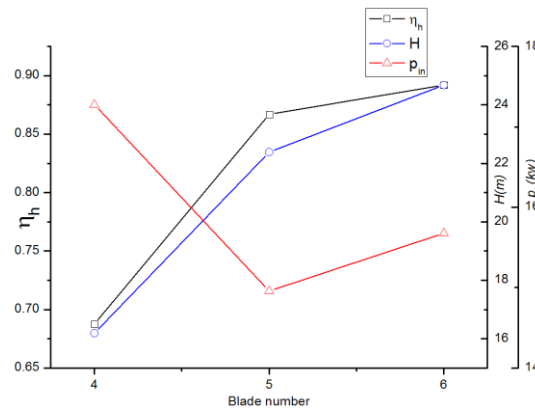


Figure 4. Hydraulic performance for pump impellers with different vane number

Figure 4 shows the hydraulic performance of pump with different blade numbers. As the blade number increases, the efficiency and head also increase. But the input power has the minimum at $z=5$.

3.2. Internal flows

Figures 5 and 6 show that the pressure distribution on the mid-span section when the wrap angle is different. As can be found, from the inlet of the impeller to the outlet, the pressure gradually increases. And with the increase of the wrap angle, the pressure in the exit area slightly increases, too, which is consistent with the result in Fig.3: the hydraulic efficiency and head increase a bit. Additionally, because of the asymmetric geometry of the volute, the pressure distribution in the passage is not periodic.

Figures 7 and 8 show the loss coefficient ζ distribution on the mid-span section and the blade surface. The loss coefficient is defined as $\zeta = \frac{2(P_1 - P_{in})}{\rho u_t^2}$, where P_1 is the local total pressure, P_{in} is the total pressure at the impeller inlet plane and u_t is the tangential velocity.[10]. With the increase of the wrap angle, the hydraulic loss in the mid-span section is significantly alleviated on the mid-span section. However, there is still severe secondary flow near the blade surface when the wrap angle is 180°. For the case, the wrap angle is 150 degree, the total hydraulic loss on mid-span section and near blades is lowest.

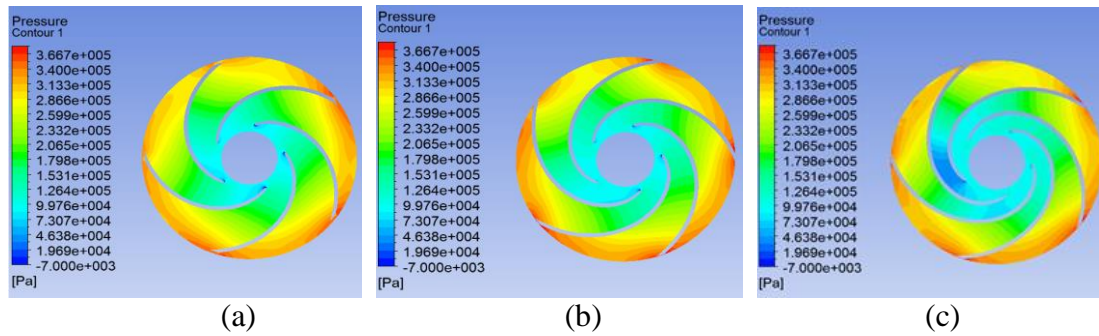


Figure 5. Static pressure distribution on the mid-span section of the impeller with different wrap angle. (a) 120° wrap angle, (b) 150° wrap angle, (c) 180° wrap angle

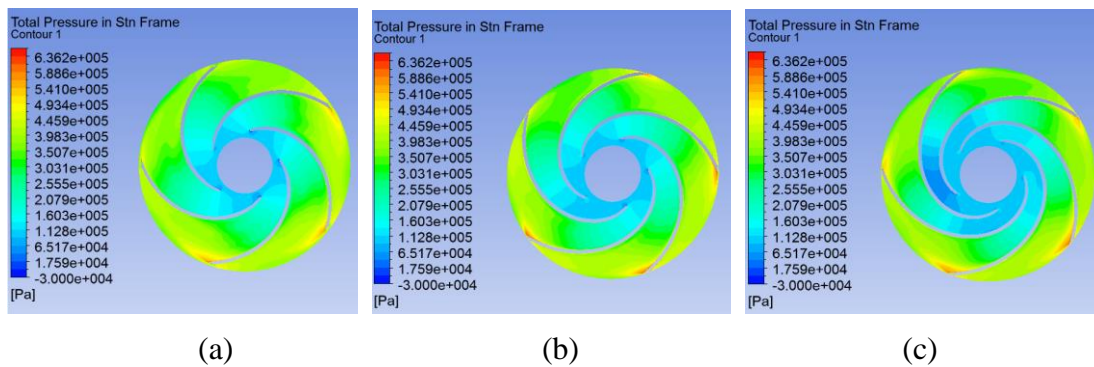


Figure 6. Total pressure distribution on the mid-span section of the impeller with different wrap angle, (a) 120° wrap angle, (b) 150° wrap angle, (c) 180° wrap angle

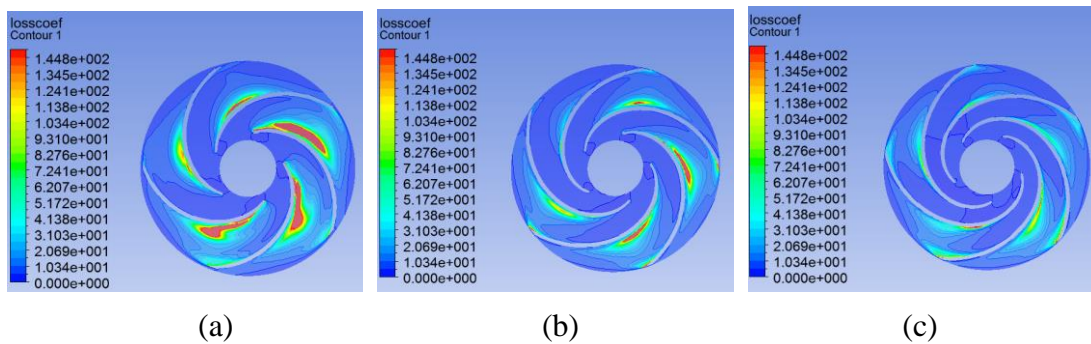


Figure 7. Loss coefficient on the mid-span section of the impeller with different wrap angle, (a) 120° wrap angle, (b) 150° wrap angle, (c) 180° wrap angle

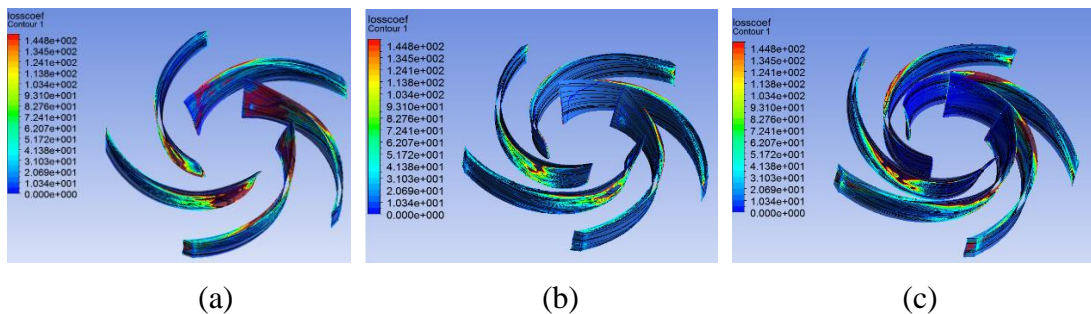


Figure 8. Loss coefficient and streamline on the blade surface with different wrap angle, (a) 120° wrap angle, (b) 150° wrap angle, (c) 180° wrap angle

Figure 9 and 10 show pressure distributions on the mid-span section when the blade number is different. These result indicate the similar pressure rise along the blade-to-blade flow channel. With the increase of the blade number, the increase of total pressure from the entrance to the exit of the impeller increases too, resulting in an increase in the hydraulic head, which is in consistent with the hydraulic performance curve as shown in figure 4. Additionally, when the blade number is 4, at the entrance part, there is an obvious low pressure area, where a severe back flow could exist, resulting in the reduction of efficiency.

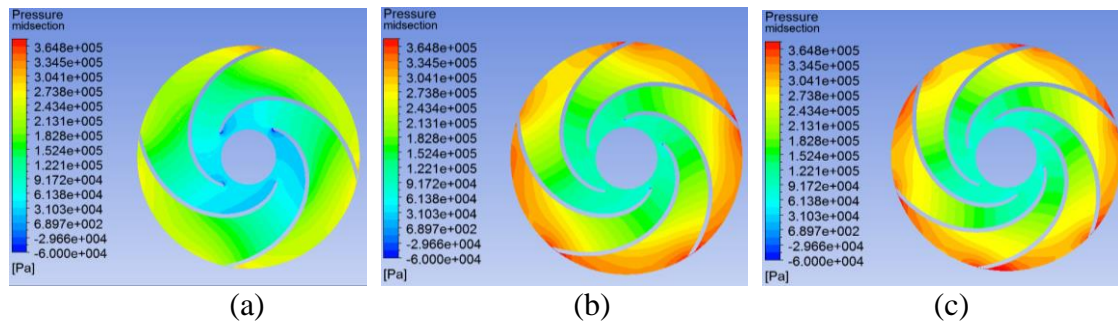


Figure 9. Static pressure distribution on the mid-span section of the impeller with different vane number, (a)4 blade number, (b) 5 blade number,(c) 6 blade number

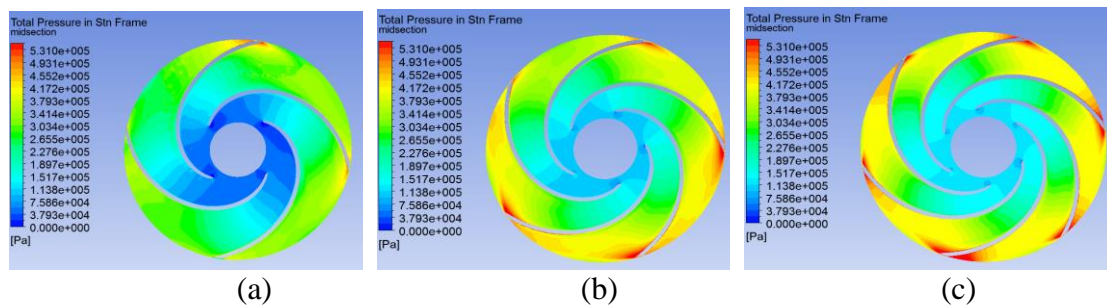


Figure 10. Total pressure distribution on the mid-span section of the impeller with different vane number, (a)4 blade number, (b) 5 blade number,(c) 6 blade number

Figure 11 and 12 show the velocity vector and loss coefficient ζ distribution on the mid-span section for the impeller with different vane number.

It is noted that when the blade number is 4, the flow separation at the entrance part is relatively serious. Additionally, for different blade number, there are some secondary flows appearing in the flow passage, such as 'a', 'b', 'c' areas, which are corresponding to the larger loss coefficient. It is noted that when the blade number is 5, the hydraulic loss is slightest.

From the loss coefficient figure, we can find that the loss majorly occurs near the pressure surface of the blade. Combined with figure 12, which is loss coefficient and streamline distribution near the blade surface, it is clear that around the pressure surface of the blade, there exist a secondary flow from the near hub area to the near shroud area. It is noted that when the blade number is 5, the hydraulic loss is slightest.

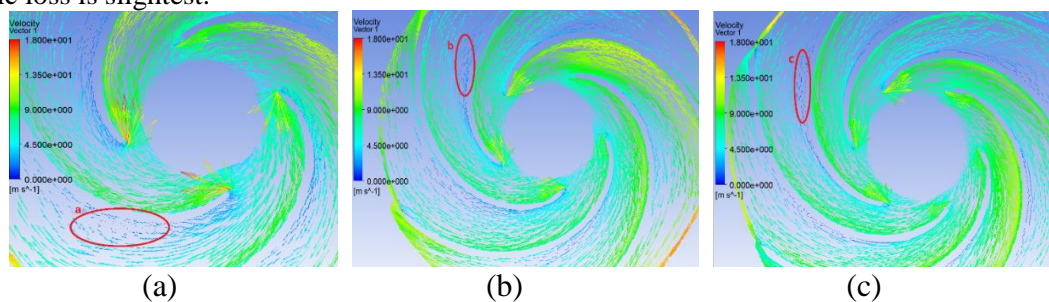


Figure 11. Velocity distribution on the mid-span section of the impeller with different vane number, (a) 4 blade number, (b) 5 blade number, (c) 6 blade number

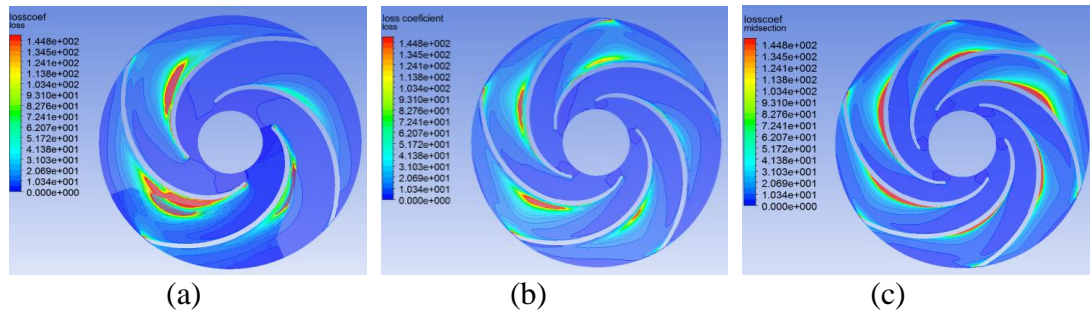


Figure 12. Loss coefficient on the mid-span section of the impeller with different vane number, (a) 4 blade number, (b) 5 blade number, (c) 6 blade number

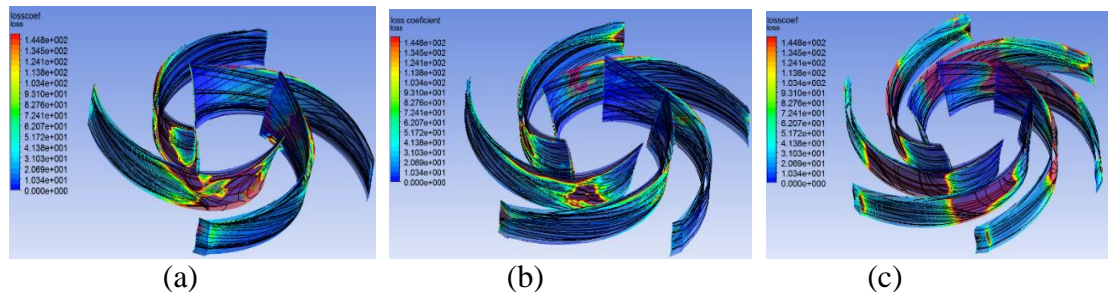


Figure 13. Loss coefficient and streamline near the blade surface with different vane number, (a) 4 blade number, (b) 5 blade number, (c) 6 blade number

3.3. Particle movement and erosion

Figure 14 shows the solid particles' volume distribution on the surface of the impeller blade under the condition of design flow. The concentration near the suction surface is relatively low, and the particles are mainly at the entrance part. While near the pressure surface, the particle distribution is much higher, concentrating in the middle part of the blade, and more obvious near the impeller hub, which is caused by the inertial force and centrifugal force. With the increase of the wrap angle, the tendency that particle concentrating near the impeller hub become more obvious.

From the erosion distribution shown in figure 15, it can be seen that with the increase of the wrap angle, the erosion condition become more severe, especially near the impeller hub on the blade pressure surface.

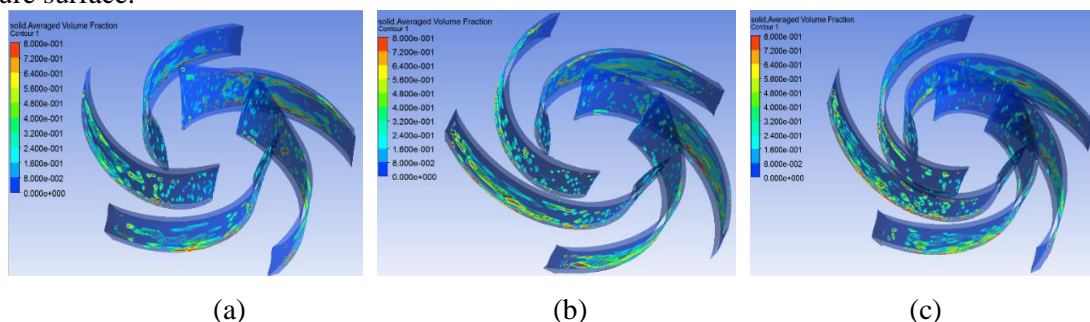


Figure 14. Particle average volume fraction near the blade, (a) 120° wrap angle, (b) 150° wrap angle, (c) 180° wrap angle

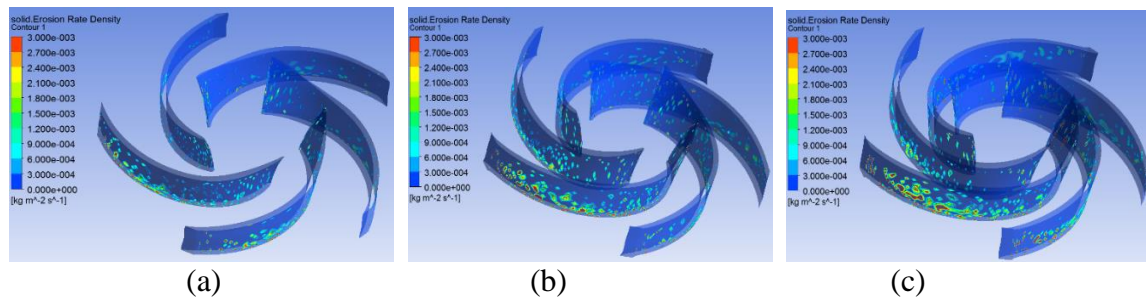


Figure 15. Erosion rate density on the blade surface, (a)120 °wrap angle, (b) 150 °wrap angle,(c) 180 °wrap angle

Figure 16 shows the erosion condition along the blade pressure surface on the mid-span section, while the erosion in the suction surface is slight and negligible. It can be seen that the erosion area is concentrated at the inlet and outlet area of the impeller vane, i.e. 0-0.2 and 0.8-1.0, and it is the most severe at the outlet area. In addition, with the vane wrap angle increases, the erosion condition in the outlet area is further intensified. Among the wrap angle of 120 degree, 150 degree and 180 degree, the highest erosion rate density is 0.011, 0.017 and 0.022 $\text{kg}/(\text{m}^2 \cdot \text{s})$ respectively.

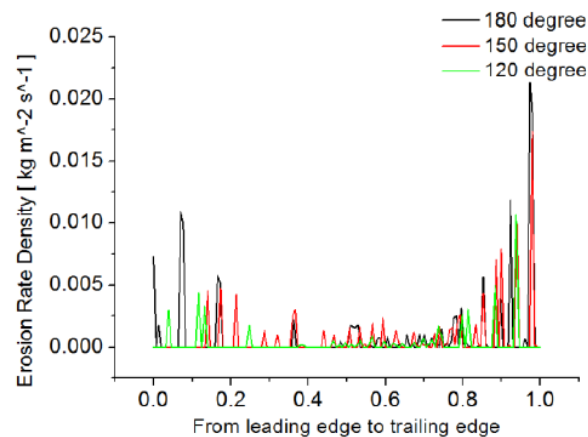


Figure 16. Erosion distribution along the midline of vane pressure surface

Table 2 shows the average collision ratio of a single particle, which is the statistics average of movement trajectories for 1,000 particles. The larger ratio means higher risk for the direct collision between the particle and the pump wall. It is known that the collision increases with the vane wrap angle, and there is the largest collision risk in the pump impeller among those pump flow passage components.

Table 2. Statistic averaged collision ratio of a single particle

	Inlet	Impeller	Volute	All domain
120°	0.05	0.75	0.56	1.36
150°	0.054	0.78	0.5732	1.4072
180°	0.062	0.869	0.5875	1.5185

It can be concluded that the erosion condition and collision risk increase with the increase of wrap angle. However, when the blade wrap angle is 150 °, there is an advantage in hydraulic efficiency over other wrap angles. Based on the balance of both the hydraulic and erosion situation, it is preferable to

choose the wrap angle of 150° .

Figure 17, 18 and 19 respectively show the averaged particle volume fraction in the mid-span section, near blade and hub area when the blade number is different. There is a concentration gradient from the suction side to the pressure side. With the increase of blade number, the particles are closer to the pressure side and also more deflected to the hub area. Which is the most remarkable when the blade number is 6.

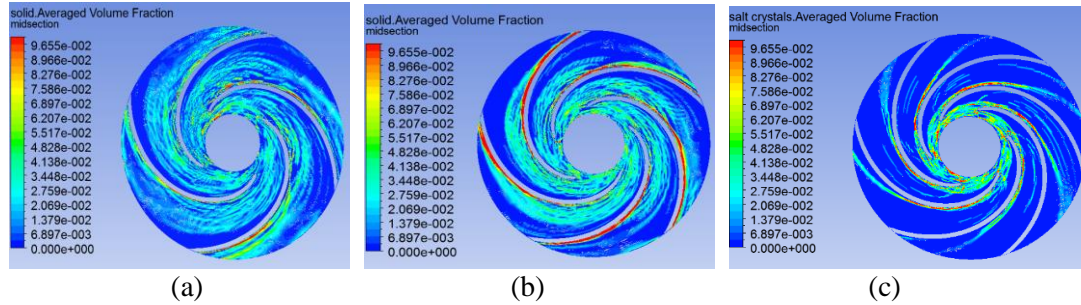


Figure 17. Particle averaged volume fraction on the mid-span section of the impeller with different vane number, (a) 4 blade number, (b) 5 blade number, (c) 6 blade number

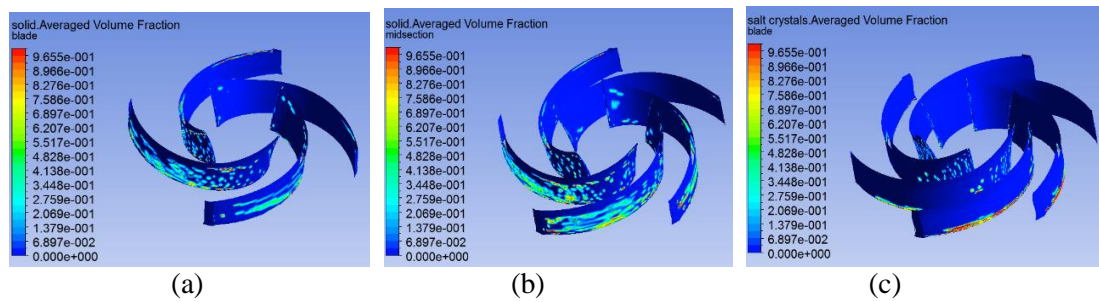


Figure 18. Particle averaged volume fraction near the blade surface, (a) 4 blade number, (b) 5 blade number, (c) 6 blade number

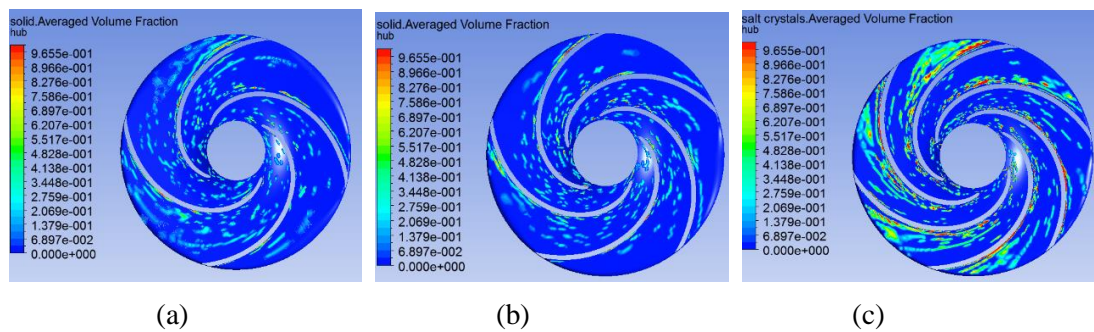


Figure 19. Particle averaged volume fraction on the hub surface, (a) 4 blade number, (b) 5 blade number, (c) 6 blade number

Figure 20 shows the erosion condition in different area of the pump. Comprehensively considering all area of the pump, when the blade number is 5, the averaged particle volume fraction is slightest, which means the erosion condition that is positively correlated with the particle fraction, is also slightest. Considering both hydraulic performance and erosion condition, it is more proper to choose a 5 blade pump.

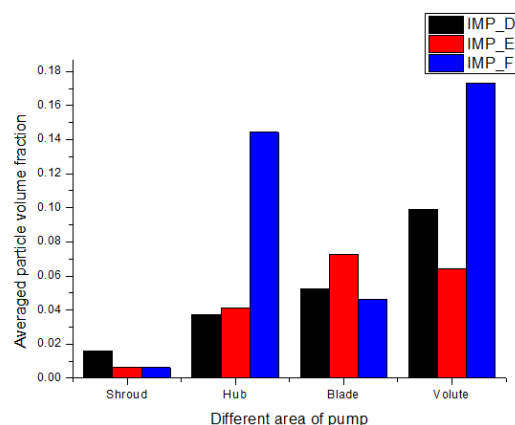


Figure 20. Averaged particle volume fraction near blade surface of different area in the salt pump

4. Conclusion

Based on the present study, the following remarks can be concluded:

The vane wrap angle and blade number are important geometries for salt pump design, which affects the hydraulic performance, collision risk and erosive wear.

For different wrap angles, the erosion condition is more severe in the inlet and outlet area of impeller vane. As the wrap angle increases, the collision risk tends to become higher, and the erosion condition is also intensified.

With the increase of blade number, the hydraulic efficiency and head become higher.

The particles move closer to the pressure side, deflecting to the impeller hub. When the wrap angle is 150° , and blade number is 5, the loss coefficient in different areas are slightest, and the erosion in the pump is better than other cases.

Acknowledgement

Tsinghua University Initiative Scientific Research Program (2016SZ0314) and Science and Technology on Water Jet Propulsion Laboratory (Project No.61422230103162223004).

References

- [1] Bing H, Tan L, Cao S L. Effects of blade number and thickness on performance of mixed-flow pumps. *Journal of Hydroelectric Engineering*, 2013, **32**(6):250-255.
- [2] Derakhshan S, Pourmahdavi M et al. Numerical shape optimization of a centrifugal pump impeller using artificial bee colony algorithm. *Computers & Fluids*, 2013, **81**: 145-151.
- [3] Zhang X, Wang Y et al. Relationship between wrap angle of impeller and performance of pump. *Transactions of The Chinese Society of Agricultural Machinery*, 2010, **41**(11):38-42.
- [4] Liu J, Xu H Y et al. Numerical simulation of erosion and particle motion trajectory in centrifugal pump. *Transactions of The Chinese Society of Agricultural Machinery*, 2008, **39**(6):54-59.
- [5] Zhao W, Ge J, Yan S et al. On Numerical value of sand erosion of centrifugal pump impeller inlet. *Journal of Gansu Sciences*, 2015.
- [6] Zhang J Q, Han Z W and Yin W. Numerical Experiment of the Solid Particle Erosion of Bionic Configuration Blade of Centrifugal Fan. *Acta Metallurgica Sinica*, 2013, **26** (1) :16-24.
- [7] Eltvik M. Sediment erosion in francis turbines. *Clinical Practice*, 2009, **11**(4):467-482.
- [8] Thapa B S. Hydraulic design of francis turbine to minimize sediment erosion. *LAP LAMBERT Academic Publishing*, 2012.
- [9] Parsons A J. Erosion and sediment transport by water on hillslopes. *Encyclopedia of Hydrological Sciences*, 2006.
- [10] Song X G, Park J H et al. Performance comparison and erosion prediction of jet pumps by using a numerical method. *Mathematical & Computer Modelling*, 2013, **57**(1-2):245-25.